1-1-2011

Schottky diode via dielectrophoretic assembly of reduced graphene oxide sheets between dissimilar metal contacts

Muhammad R. Islam
University of Central Florida

Daeha Joung
University of Central Florida

Saiful I. Khondaker
University of Central Florida

Schottky diode via dielectrophoretic assembly of reduced graphene oxide sheets between dissimilar metal contacts

To cite this article: Muhammad R Islam *et al* 2011 *New J. Phys.* **13** 035021

New Journal of Physics
The open-access journal for physics

Schottky diode via dielectrophoretic assembly of reduced graphene oxide sheets between dissimilar metal contacts

Muhammad R Islam[1,2], **Daeha Joung**[1,2] and **Saiful I Khondaker**[1,2,3,4]

[1] Nanoscience Technology Center
[2] Department of Physics
[3] School of Electrical Engineering and Computer Science, University of Central Florida, Orlando, FL 32826, USA
E-mail: saiful@mail.ucf.edu

New Journal of Physics **13** (2011) 035021 (10pp)
Received 7 December 2010
Published 23 March 2011
Online at http://www.njp.org/
doi:10.1088/1367-2630/13/3/035021

Abstract. We demonstrate the fabrication of reduced graphene oxide (RGO) Schottky diodes via dielectrophoretic (DEP) assembly of RGO between two dissimilar metal contacts. Titanium (Ti) was used to make a Schottky contact, while palladium (Pd) was used to make an Ohmic contact. From the current–voltage characteristics, we obtain rectifying behavior with a rectification ratio of up to 600. The ideality factor was high (4.9), possibly due to the presence of a large number of defects in the RGO sheets. The forward biased turn-on voltage was 1 V, whereas the reverse biased breakdown voltage was −3.1 V, which improved further upon mild annealing at 200 °C and can be attributed to an increase in the work function of RGO due to annealing.

Contents

[4] Author to whom any correspondence should be addressed.

1. Introduction

Owing to its exceptional electrical and photonic properties, graphene is considered to be a promising building block for future generations of electronic and optoelectronic devices [1]–[4]. For the large-scale fabrication of graphene-based devices, exfoliation of graphite into individual graphene sheets in large quantities is required. Reduced graphene oxide (RGO) sheets have been extensively investigated as an attractive pathway to produce large quantities of graphene sheets in solution [5]–[25]. RGO offers tunability of electronic and optical properties via controlling the reduction process through the chemical and/or thermal route [5]–[17], [20]–[25]. In addition, the ease of material processing, low cost of synthesis, mechanical flexibility and ability to make composite materials [18, 19] make them an attractive candidate for fabricating various functional devices. For example, RGO has already been used for the fabrication of field effect transistors [15]–[17], photodetectors [20], organic solar cells [21]–[25] and chemical/biological sensors [26]–[31]. Another fundamental building block of an electronic circuit is a diode. From the beginning of semiconductor device developments, the diode played a critical role in the understanding of metal semiconductor interface and found many applications in electronics and optoelectronics. Compared to the p–n diode, the Schottky diode generally exhibits a faster switching speed and low forward resistance, and is suitable for high-speed rectification devices [32]. In addition, the Schottky diode was also found to be useful for gas-sensing applications [33, 34]. The Schottky diode is typically made by connecting one end of a p- (or n)-type semiconducting material with a metal of high (or low) work function that gives the Ohmic contact, whereas the other end is connected to a metal with lower (or higher) work function giving the Schottky contacts. Recent attempts at fabrication of the Schottky diode with graphene show that pristine graphene, which is a semimetal, has to be converted to a semiconductor via controlled exposure of oxygen plasma [35]. Since RGO has a lot of localized graphene domains [9, 36], which creates a band gap, it can readily be used for the fabrication of a Schottky diode. In addition, fabrication of the Schottky diode with RGO is advantageous as it allows high-throughput fabrication of devices.

In this paper, we demonstrate fabrication and characterization of RGO Schottky diodes with good rectification behavior. The RGO sheets suspended in water were assembled between a prefabricated dissimilar metal source and drain contacts. Titanium (Ti) with a work function lower than RGO was used to make a Schottky contact, whereas palladium (Pd) with a work function larger than RGO was used to make the Ohmic contact. The RGO sheets were then assembled using ac dielectrophoresis (DEP). From the current–voltage (I–V) characteristics, we obtained rectifying behavior with a rectification ratio of up to 600. The ideality factor (4.9) was found to be higher than the ideal diode possibly due to the presence of a large number of defects in the RGO sheets. The forward biased turn-on voltage was 1 V, whereas the reverse biased breakdown voltage was −3.1 V, which improved further upon mild annealing at 200 °C that can be attributed to an increase in work function of RGO due to annealing. Our demonstration of a RGO Schottky diode via DEP creates another fundamental device building block involving RGO for future nanoelectronic applications.

2. Experimental

RGO sheets used in this study were obtained via chemical reduction of individual graphene oxide (GO) sheets. The individual GO sheets in powder form were obtained from Cheaptubes

Inc (http://www.cheaptubes.com). 2 mg of the GO powder was added to 50 ml of deionized water in a vial. The pH of the solution was adjusted to 11 by using an aqueous solution of ammonia. Then 2 μl of hydrazine (35% DMF) solution was added to the mixture. The vial containing the mixture was then placed in a water bath kept at $\sim$100 °C, stirred using a magnetic stirrer for 1 h and then cooled to room temperature. X-ray photoelectron spectroscopy (XPS), atomic force microscopy (AFM) and Raman spectroscopy were used to characterize the obtained RGO sheets. XPS analysis was performed using a Physical Electronics 5400 ESCA system. AFM images were taken on a Dimension 3100 scanning probe microscope (Vecco Instruments Inc). For AFM study, the RGO suspension was spin-coated on a mica substrate. Images were obtained using tapping mode and collected under ambient conditions at 60% relative humidity and 25.8 °C with a scanning rate of 0.5 Hz. We used a Renishaw *inVia* micro-Raman spectrometer with 514 nm excitation, $\sim$1 μm spot size and $\sim$1 mW power for Raman spectroscopy.

The Schottky diodes were fabricated as follows. First, the electrodes were fabricated using a combination of optical and electron beam lithography (EBL). Then the RGO sheets were assembled between the electrodes via DEP. The device platform was a highly p-doped Si wafer with a thermally grown 250 nm thick SiO_2 on its surface. Larger size contact pads and position alignment markers were fabricated via optical lithography using double layer resists (LOR 3A/Shipley 1813), developed in CD26, followed by thermal evaporation of chromium (Cr) (5 nm) and Au (45 nm) and then standard lift-off. The smaller electrode patterns with dissimilar metals were done using two steps of EBL writing. First, Ohmic contact was defined by EBL and deposition of 25 nm Pd using single-layer poly(methyl methacrylate) (PMMA) resists, and then developed in (1 : 3) methyl isobutyl ketone : isopropyl alcohol (MIBK : IPA) followed by lift-off. Another layer of EBL was then implemented to define the Schottky contact (Ti) following the same process as Pd. The gap between the two electrodes was 200 nm. Prior to the RGO assembly, the electrodes were treated in oxygen plasma for 15 min to remove any residual organics. We also attempted to use Au–Cr electrodes; however, we did not obtain good diode characteristics. For control experiments, we also fabricated devices with Au–Au and Pd–Pd contact and did not obtain any Schottky behavior.

An ac DEP was used to assemble RGO sheets between the prefabricated Pd and Ti electrodes. The process was similar to our recent reports of high yield RGO FET fabrication using Au metal electrodes [17]. DEP has recently been used to fabricate devices using one-dimensional (1D) and 0D nanostructures as well [37]–[43]. In brief, a 2 μl drop of RGO solution was cast on the chips containing the electrodes. An ac voltage of 3 V peak to peak at 1 MHz was applied between the electrodes for 10–15 s. The ac voltage generated a time-averaged DEP force between the electrode gap, which can be expressed as $F_{\mathrm{DEP}} = (p \cdot \nabla)E$, where p is the dipole moment of the polarizable object and $\boldsymbol{E}$ is the non-uniform electric field set up by the ac voltage [17, 44]. The strong electric field gradient caused the RGO sheets to align along the field direction and assemble between the Pd–Ti electrodes. After the assembly, the solution droplet was blown off by a stream of nitrogen gas flow. The room-temperature electronic transport measurements of the fabricated devices were carried out in a probe station at ambient environment. The measurements were performed using a Keithley 2400 source-meter and a current preamplifier (DL 1211) capable of measuring sub-pA signal interfaced with the LABVIEW program. A total of 16 devices were investigated.

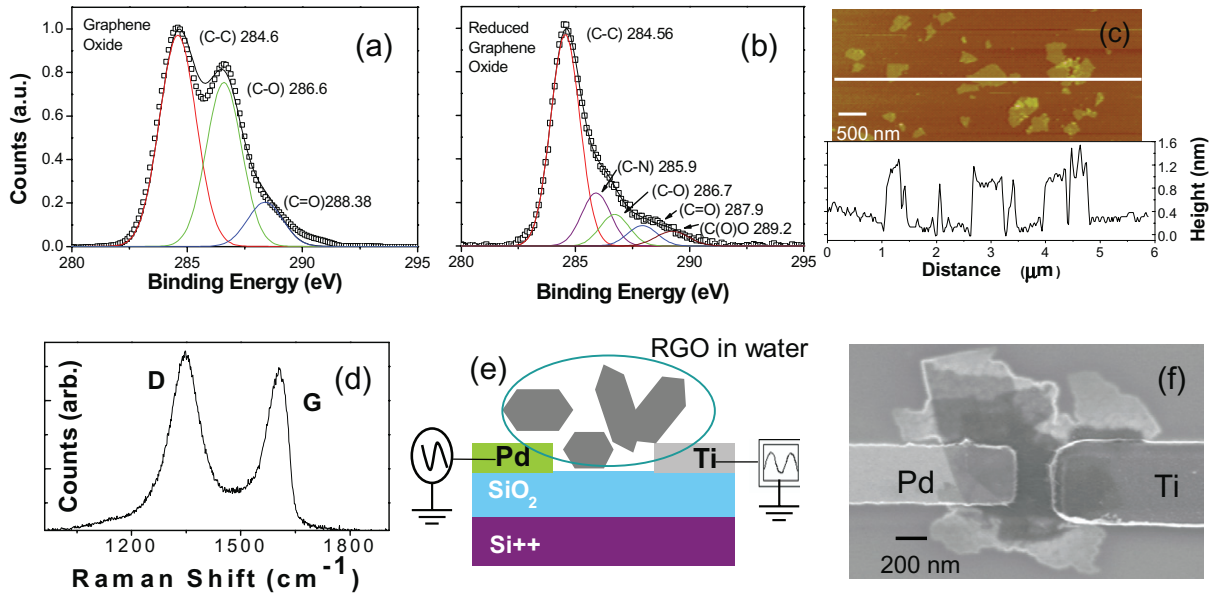

Figure 1. (a) XPS spectra of a GO thin film on Si/SiO_2 substrate. (b) XPS data for a RGO thin film. (c) Tapping-mode AFM image of RGO sheets with a height profile indicating that the majority of the sheets are single layer. (d) Raman spectra of RGO sheet. (e) Schematic diagram of the DEP assembly setup for RGO Schottky diode with Ti as Schottky and Pd as Ohmic contact. (f) SEM image of a DEP assembled RGO diode device.

3. Results and discussion

Figure 1(a) shows the XPS data taken on a thin film of GO dispersed on Si/SiO_2. Here we can see the three components of carbon-based atom in different functional groups of GO: (i) the non-oxygenated C–C bond (284.6 eV), (ii) C–O bond (286.6 eV) and (iii) the C=O bond (288.38 eV). Figure 1(b) shows the XPS data after reduction (RGO) in hydrazine. The peaks for oxygen functional groups in RGO were significantly reduced. An additional peak also appeared at 285.9 eV corresponding to the C in the C–N bond. This also implies that the oxygen in the GO is considerably removed by the reduction process and that nitrogen is now present due to the hydrazine treatment. The ratio of O_{1s}/C_{1s} peaks is about 0.14, indicating good reduction efficiency, and it is comparable to previous studies [14, 45]. Figure 1(c) displays a tapping-mode AFM image of the RGO sheets along with their height analysis. The lateral dimension of our RGO sheets varies from 0.2–2 μm. The line graph represents the thickness of the RGO sheets. Approximately 70% of the sheets displayed a height of 1.0 ± 0.2 nm.

The Raman spectroscopy was used for identifying the orderliness of the RGO crystal structure. Usually the G-band (sp^2) corresponds to orderliness and the D-band corresponds to disorderliness (sp^3) of the material [36]. The Raman spectrum of our RGO sheets is presented in figure 1(d). It exhibits the D-band peak at 1346 cm^{-1} and the G-band peak at 1604 cm^{-1}. The broader D-band with higher relative intensities compared to that of the G-band indicates the higher disorderliness in the RGO sheets. The ratio $I_D : I_G$ is about 1.10, from which we obtain an average graphitic domain size of about 4 nm using an empirical Tunistra–Koening relation [46].

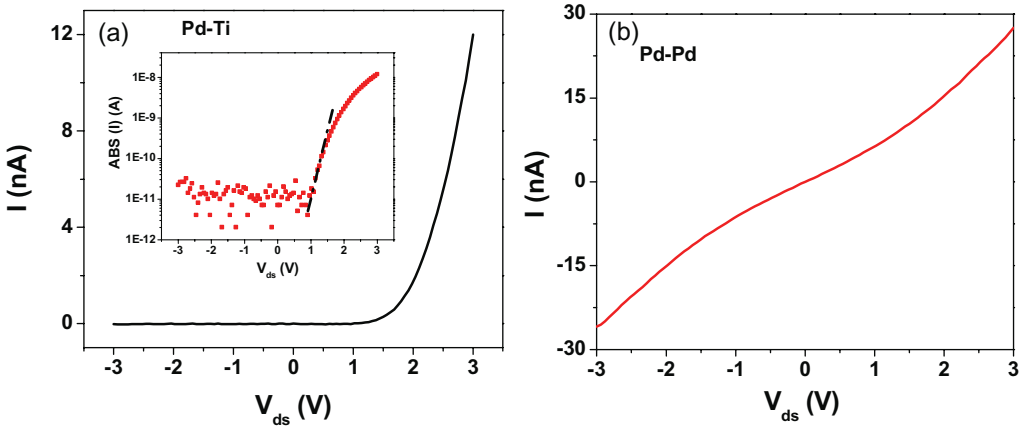

Figure 2. (a) A representative current–voltage (I–V) characteristics curve of a Ti/RGO/Pd Schottky diode assembled via DEP showing rectifying behavior. Inset: the semi-log plot of the absolute magnitude of current versus voltage of the device. The black line represents the linear fitting of the diode equation from which we obtain the ideality factor as $n = 4.9$. (b) I–V curve of a control RGO device with Pd–Pd metal contact. No Schottky behavior can be seen.

After the DEP assembly of the RGO sheets between Pd and Ti electrodes, the device yield was tested using a scanning electron microscope (SEM). Figure 1(e) shows a diagram of the DEP setup. Figure 1(f) shows an SEM image of one of our representative devices. From the AFM height analysis (not shown here) of this device, we found that up to eight layers of RGO are assembled in the channel. The thickness is lower at the edges with one or two layers of graphene sheet near the edge, while the thickness is higher in the middle of the channel due to the overlap of several individual sheets or folding of the sheets. Our chip had 16 electrodes pairs, all of which were bridged by a few layers of RGO sheets during the DEP assembly, giving a 100% device yield.

Figure 2(a) shows the current–voltage (I–V) characteristics of one of our representative devices measured at room temperature with a Ti electrode grounded and a Pd electrode swept from −3 to +3 V. The curve is nonlinear and asymmetric. The device did not show any significant reverse biased breakdown (or reverse leakage current) for up to −3 V. The device gives a high rectification ($I_{\text{forward}}/I_{\text{reverse}}$) ratio of ~ 600 within these voltage ranges. Figure 2(b) show the I–V curve of one of our control samples with Pd–Pd contact. In contrast to Pd–Ti contact, no Schottky behavior is observed. From this, we conclude that the observed Schottky diode with a good rectification is a result of carefully chosen dissimilar metal contacts with RGO.

For a Schottky diode, the I–V relation can be expressed as $I = I_0[\exp(eV/nkT) - 1]$, where e is the charge of electron, k is the Boltzman constant, n is the ideality factor, T is the absolute temperature and I_0 is the saturation current. Our diode follows this behavior with $n = 4.9$ in the forward biased region obtained by plotting the log I against V and using the equation $n = e/kT[\mathrm{d}V/\mathrm{d}(\ln I)]$ [32]. This is shown in the inset of figure 2(a). The value of n is higher than what is expected for an ideal diode ($n = 1$). Similarly, a high value of n was also reported for Schottky diodes based on disordered organic semiconductors and has been attributed to accelerated recombination of electrons and holes in the depletion region and the presence of an interfacial layer or surface states [47]–[52]. In addition, it was noted that when

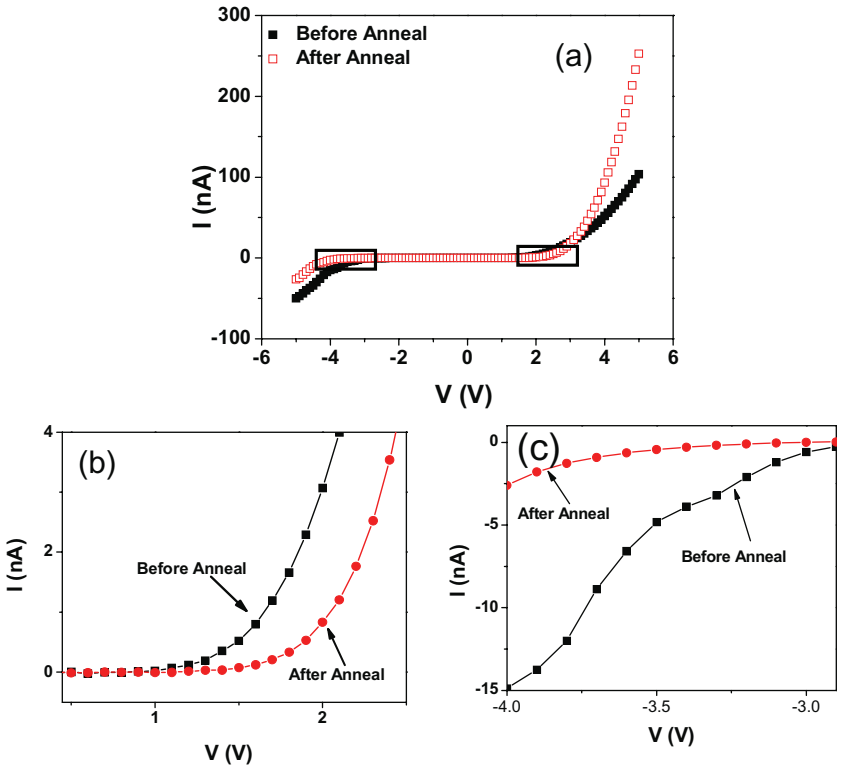

Figure 3. (a) *I–V* curve of a RGO Schottky diode before and after annealing. (b) Magnified view of the *I–V* characteristics in the forward biased regime, which show the turn-on voltage increased from 1 to 1.5 V upon annealing. (c) Magnified view of the *I–V* curve in the reverse biased regime. The breakdown voltage changed from −3.1 to −3.6 V upon annealing.

the charge transport is dominated by space charge limited conduction, it is common to observe a higher value of n [49]–[52]. Recently, we reported SCLC behavior in RGO devices connected to a gold electrode arising from a large amount of structural disorder and trap states due to oxidized carbon atoms, point defects and topological defects [53]. Therefore, a high value of n in our RGO Schottky diode is not surprising.

We have also examined the affect of annealing on the properties of our RGO Schottky diodes. The annealing was done in an argon (Ar) and/hydrogen (H_2) atmosphere inside a tube furnace. A flow of 200 cc min^{-1} of Ar and 2000 cc min^{-1} H_2 was initiated and the gases were kept flowing for a few minutes to purge the system. The furnace was then heated to 200 °C for 1 h and then turned off. During cool down of the furnace, both Ar and H_2 flows were maintained until the furnace reached room temperature. Figure 3(a) shows the *I–V* curve measured between −5 and +5 V of the same device before and after thermal annealing. The filled squares represent before annealing, whereas the open squares represent after thermal annealing. The effect of annealing on the diode characteristics can be more clearly seen in figures 3(b) and (c). From figure 3(b), we see that the turn-on voltage has been changed from 1 to 1.5 V, whereas figure 3(c) shows that the reverse biased breakdown voltage has been changed from −3.1 to −3.6 V after annealing. A similar trend has been observed for all of the devices that we investigated.

The diode behavior of the RGO device with or without annealing can be explained using the band diagram shown in figure 4. In previous studies, the work function of RGO has been

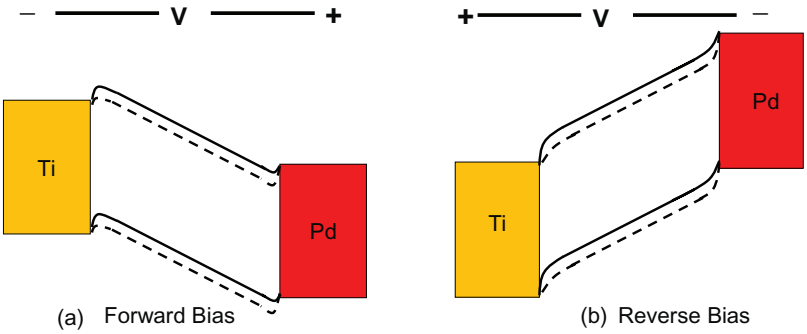

Figure 4. Energy band diagram of RGO Schottky diode before annealing (dashed line) and after annealing (solid line) under (a) forward and (b) reverse biased condition. A Schottky junction is formed between the RGO and Ti, and a bending of energy band occurs. After annealing, the work function of RGO increases, causing more bending at the Schottky contact.

reported to vary between 4.3 and 4.7 eV [54, 55]. It was also reported that the work function of RGO increases with increasing reduction efficiency or the increase in the C–C to C–O ratio [56]. In our previous study involving DEP assembled RGO with a Au electrode, we showed that mild annealing reduces the sample resistance and improves the on-current of the field effect transistors [17]. In order to explain this, we carried out XPS analysis before and after annealing and found that the C–C to C–O ratio increased from 8 to 14 on annealing at 200 °C [17]. This implies that mild annealing of the device increases the work function of RGO. This is shown in the band diagram of RGO in figure 4, where the dashed line represents RGO before annealing, while the solid line represents RGO after annealing. Ti, having a work function of ~ 4.33 eV, makes a Schottky contact with RGO, whereas Pd, having a work function of ~ 5.5 eV, makes an Ohmic contact with RGO. The work function difference between RGO and Ti creates a contact potential barrier (V_c), which leads to bending of the energy band and prevents the flow of holes from RGO to Ti.

In the forward biased regime, when a potential V_f (or bias voltage) is applied, the V_c is reduced to $V_c - V_f$; this reduces the bending at the Schottky junction and holes start to diffuse through the barrier, giving forward current. On the other hand, in the reverse biased regime, the reverse biased potential (V_r) increases the contact potential to $V_c + V_r$ (shown in figure 4(b)), which causes a blockage of hole transportation. On annealing the RGO device, the work function of RGO increases, and so the value of V_c between Ti and RGO also increases, causing a larger bending of energy band between RGO and Ti. That is why a higher turn-on voltage is needed to overcome the contact barrier on annealing in the forward biased regime and the breakdown voltage decreased in the reverse biased regime.

4. Conclusions

In conclusion, we demonstrated fabrication of RGO Schottky diodes via DEP assembly of RGO sheets between Ti and Pd electrodes. The device shows good rectification behavior with a rectification ratio of up to 600. The ideality factor of the diodes was high due to the presence of disorder in the RGO sheets. A mild thermal annealing causes an increase in the turn-on

voltage in the forward biased regime and a decrease in the reverse breakdown voltage in the reverse biased regime. This can be explained by considering the fact that the work function of a RGO increased due to annealing. Our demonstration of a RGO Schottky diode via DEP creates another fundamental device building block involving RGO for future nanoelectronic applications.

Acknowledgment

This work was partially supported by the US NSF under grant no. ECCS 0748091.

References

[1] Novoselov K S, Geim A K, Morozov S V, Jiang D, Zhang Y, Dubonos S V, Grigorieva I V and Firsov A A 2004 Electric field effect in atomically thin carbon films *Science* **306** 666–9
[2] Zhang Y, Tan Y W, Stormer H L and Kim P 2005 Experimental observation of the quantum Hall effect and Berry's phase in graphene *Nature* **438** 201–4
[3] Geim A K and Novoselov K S 2007 The rise of graphene *Nat. Mater.* **6** 183–91
[4] Wang F, Zhang Y, Tian C, Girit C, Zettl A, Crommie M and Shen Y R 2008 Gate-variable optical transition in graphene *Science* **320** 206–9
[5] Park S and Ruoff R S 2009 Chemical methods for the production of graphenes *Nat. Nanotechnol.* **4** 217–24
[6] Stankovich S, Dikin D A, Dommett G H B, Kohlhaas K M, Zimney E J, Stach E A, Piner R D, Nguyen S T and Ruoff R S 2006 Graphene-based composite materials *Nature* **442** 282–6
[7] Schniepp H C, Li J L, McAllister M J, Sai H, Herrera-Alonso M, Adamson D H, Prudhomme R K, Car R, Saville D A and Aksay I A 2006 Functionalized single graphene sheets derived from splitting graphite oxide *J. Phys. Chem.* B **110** 8535–9
[8] Stankovich S, Piner R D, Nguyen S T and Ruoff R S 2006 Synthesis and exfoliation of isocyanate-treated graphene oxide nanoplatelets *Carbon* **44** 3342–7
[9] Gomez-Navarro C, Weitz R T, Bittner A M, Scolari M, Mews A, Burghard M and Kern K 2007 Electronic transport properties of individual chemically reduced graphene oxide sheets *Nano Lett.* **7** 3499–503
[10] Jung I, Dikin D A, Piner R D and Ruoff R S 2008 Tunable electrical conductivity of individual graphene oxide sheets reduced at 'low' temperatures *Nano Lett.* **8** 4283–7
[11] Li D, Muller M B, Gilje S, Kaner R B and Wallace G G 2008 Processable aqueous dispersions of graphene nanosheets *Nat. Nanotechnol.* **3** 101–5
[12] Tung V C, Allen M J, Yang Y and Kaner R B 2009 High-throughput solution processing of large-scale graphene *Nat. Nanotechnol.* **4** 25–9
[13] Mattevi C, Eda G, Agnoli S, Miller S, Mkhoyan K A, Celik O, Mastrogiovanni D, Granozzi G, Garfunkel E and Chhowalla M 2009 Evolution of electrical, chemical, and structural properties of transparent and conducting chemically derived graphene thin films *Adv. Funct. Mater.* **19** 2577–83
[14] Yang D *et al* 2009 Chemical analysis of graphene oxide films after heat and chemical treatments by x-ray photoelectron and micro-Raman spectroscopy *Carbon* **47** 145–52
[15] Gilje S, Han S, Wang M, Wang K L and Kaner R B 2007 A chemical route to graphene for device applications *Nano Lett.* **7** 3394–8
[16] Eda G, Fanchini G and Chhowalla M 2008 Large-area ultrathin films of reduced graphene oxide as a transparent and flexible electronic material *Nat. Nanotechnol.* **3** 270–4
[17] Joung D, Chunder A, Zhai L and Khondaker S I 2010 High yield fabrication of chemically reduced graphene oxide field effect transistor by dielectrophoresis *Nanotechnology* **21** 165202

[18] Lightcap I V, Kosel T H and Kamat P V 2010 Anchoring semiconductor and metal nanoparticles on a two-dimensional catalyst mat. storing and shuttling electrons with reduced graphene oxide *Nano Lett.* **10** 577–83
[19] Chunder A, Pal T, Khondaker S I and Zhai L 2010 Reduced graphene oxide/copper phthalocyanine composite and its optoelectrical properties *J. Phys. Chem.* C **114** 15129–35
[20] Ghosh S, Sarker B K, Chunder A, Zhai L and Khondaker S I 2010 Position dependent photodetector from large area reduced graphene oxide thin films *Appl. Phys. Lett.* **96** 163109
[21] Eda G, Lin Y Y, Miller S, Chen C W, Su W F and Chhowalla M 2008 Transparent and conducting electrodes for organic electronics from reduced graphene oxide *Appl. Phys. Lett.* **92** 233305
[22] Wang X, Zhi L and Mullen K 2008 Transparent, conductive graphene electrodes for dye-sensitized solar cells *Nano Lett.* **8** 323–7
[23] Liu Q, Liu Z, Zhang X, Zhang N, Yang L, Yin S and Chen Y 2008 Organic photovoltaic cells based on an acceptor of soluble graphene *Appl. Phys. Lett.* **92** 223303
[24] Liu Z, Liu Q, Huang Y, Ma Y, Yin S, Zhang X, Sun W and Chen Y 2008 Organic photovoltaic devices based on a novel acceptor material: graphene *Adv. Mater.* **20** 3924–30
[25] Wu J, Becerril H A, Bao Z, Liu Z, Chen Y and Peumans P 2008 Organic solar cells with solution-processed graphene transparent electrodes *Appl. Phys. Lett.* **92** 263302
[26] Robinson J T, Perkins F K, Snow E S, Wei Z and Sheehan P E 2008 Reduced graphene oxide molecular sensors *Nano Lett.* **8** 3137–40
[27] Mohanty N and Berry V 2008 Graphene-based single-bacterium resolution biodevice and DNA transistor: interfacing graphene derivatives with nanoscale and microscale biocomponents *Nano Lett.* **8** 4469–76
[28] Fowler J D, Matthew J, Allen M J, Tung V C, Yang Y, Kaner R B and Weiller B H 2009 Practical chemical sensors from chemically derived graphene *ACS Nano* **3** 301–6
[29] Arsat R, Breedon M, Shafiei M, Spizziri P G, Gilje S, Kaner R B, Kalantar-zadeh K and Wlodarski W 2009 Graphene-like nano-sheets for surface acoustic wave gas sensor applications *Chem. Phys. Lett.* **467** 344–7
[30] Zhou M, Zhai Y and Dong S 2009 Electrochemical sensing and biosensing platform based on chemically reduced graphene oxide *Anal. Chem.* **81** 5603–13
[31] Lu G, Ocola L E and Chen J 2009 Gas detection using low-temperature reduced graphene oxide sheets *Appl. Phys. Lett.* **94** 083111
[32] Sze S M 1981 *Physics of Semiconductor Device* 2nd edn (New York: Wiley)
[33] Shafiei M, Spizzirri P G, Arsat R, Yu J, Plessis J D, Dubin S, Kaner R B, Kalantar-zadeh K and Wlodarski W 2010 Platinum/graphene nanosheet/SiC contacts and their application for hydrogen gas sensing *J. Phys. Chem.* C **114** 13796–801
[34] Yu J, Ippolito S J, Wlodarski W, Strano M and Kalantar-zadeh K 2010 Nanorod based Schottky contact gas sensors in reversed bias condition *Nanotechnology* **21** 265502
[35] Nourbakhsh A, Cantoro M, Hadipour A, Vosch T, Veen M H V D, Heyns M M, Sels B F and Gendt S D 2010 Modified, semiconducting graphene in contact with a metal: characterization of the Schottky diode *Appl. Phys. Lett.* **97** 163101
[36] Joung D, Zhai L and Khondaker S I 2011 Coulomb blockade and hopping conduction in graphene quantum dots array in press (arXiv:cond-mat1101.4040)
[37] Stokes P and Khondaker S I 2008 Local-gated single-walled carbon nanotube field effect transistors assembled by AC dielectrophoresis *Nanotechnology* **17** 175202
[38] Stokes P and Khondaker S I 2010 High quality solution processed carbon nanotube transistors assembled by AC dielectrophoresis *Appl. Phys. Lett.* **96** 083110
[39] Stokes P and Khondaker S I 2010 Evaluating defects in solution processed carbon nanotube devices via low temperature transport spectroscopy *ACS Nano* **4** 2659–66
[40] Khondaker S I 2004 Fabrication of nanoscale device using individual colloidal gold nanoparticle *IEE Proc. Circuits Devices Syst. (Special Issue in Nanoelectronics)* **151** 457–60

[41] Khondaker S I and Yao Z 2002 Fabrication of nanometer spaced electrodes using gold nanoparticles *Appl. Phys. Lett.* **81** 4613
[42] Khondaker S I, Luo K and Yao Z 2010 Fabrication of single-electron transistors using dielectrophoretic trapping of individual gold nanoparticles *Nanotechnology* **21** 095204
[43] Sadek A Z, Zhang C, Hu Z, Partridge J G, McCulloch D G, Wlodarski W and Kalantar-zadeh K 2010 Uniformly dispersed Pt−Ni nanoparticles on nitrogen-doped carbon nanotubes for hydrogen sensing *J. Phys. Chem.* C **114** 238–42
[44] Jones T B 1995 *Electromechanics of Particles* (Cambrige: Cambrige University Press)
[45] Stankovich S, Piner R D, Chen X, Wu N, Nguyen S T and Ruoff R S 2006 Stable aqueous dispersions of graphitic nanoplatelets via the reduction of exfoliated graphite oxide in the presence of poly(sodium 4-styrenesulfonate) *J. Mater. Chem.* **16** 155–8
[46] Tuinstra F and Koenig J L 1970 Raman spectrum of graphite *J. Chem. Phys.* **53** 1126–30
[47] Gupta R, Mishra S C K, Malhotra B D, Beladakere N N and Chandra S 1991 Metal/semiconductor polymer Schottky device *Appl. Phys. Lett.* **58** 51–2
[48] Martinez O, Bravo A G and Pinto N J 2009 Fabrication of Poly(vinylidene fluoride−trifluoroethylene)/ Poly(3,4-ethylenedioxythiophene)−polystyrene sulfonate composite nanofibers via electrospinning, *Macromolecules* **42** 7924–9
[49] Taylor D M and Gomes H L 1995 Electrical characterization of the rectifying contact between aluminium and electrodeposited poly(3-methylthiophene) *J. Phys. D: Appl. Phys.* **28** 2554–68
[50] Tagmouti S, Outzourhit A, Oueriagli A, Khaidar M, Elyacoubi M, Evrard R and Ameziane E L 2000 Electrical characteristics of W/P3MT/Pt diodes *Thin Solid Films* **379** 272–8
[51] Yakuphanoglu F, Basaran E, Senkal B F and Sezer E 2006 Electrical and optical properties of an organic semiconductor based on polyaniline prepared by emulsion polymerization and fabrication of Ag/Polyaniline/n-Si Schottky diode *J. Phys. Chem.* B **110** 16908–13
[52] Giulianini M, Waclawik E R, Bell J M and Motta N 2009 Current-voltage characteristics of poly(3-hexylthiophene) diodes at room temperature *Appl. Phys. Lett.* **94** 083302
[53] Joung D, Chunder A, Zhai L and Khondaker S I 2010 Space charge limited conduction with exponential trap distribution in reduced graphene oxide sheets *Appl. Phys. Lett.* **97** 093105
[54] Matyba P, Yamaguchi H, Eda G, Chhowalla M, Edman L and Robinson N D 2010 Graphene and mobile ions: the key to all-plastic, solution-processed light-emitting devices *ACS Nano* **4** 637–42
[55] Lin Y, Zhang K, Chen W, Liu Y, Geng Z, Zeng J, Pan N, Yan L, Wang X and Hou J G 2010 Dramatically enhanced photoresponse of reduced graphene oxide with linker-free anchored CdSe nanoparticles *ACS Nano* **4** 3033–8
[56] Shin H J *et al* 2009 Efficient reduction of graphite oxide by sodium borohydride and its effect on electrical conductance *Adv. Funct. Mater.* **19** 1987–92